Eyetracker-based gaze correction for robust mapping of population receptive fields

A. Hummer [a], M. Ritter [b], M. Tik [a], A.A. Ledolter [b], M. Woletz [a], G.E. Holder [c,d], S.O. Dumoulin [e,f], U. Schmidt-Erfurth [b], C. Windischberger [a,*]

[a] MR Centre of Excellence, Center for Medical Physics and Biomedical Engineering, Medical University of Vienna, Währinger Gürtel 18-20, 1090 Vienna, Austria
[b] Department of Ophthalmology and Optometry, Medical University of Vienna, Währinger Gürtel 18-20, 1090 Vienna, Austria
[c] Institute of Ophthalmology, University College London, 11-43 Bath Street, London, EC1V 2PD, UK
[d] Moorfields Eye Hospital, 162 City Road, London, EC1V 9EL, UK
[e] Experimental Psychology, Helmholtz Institute, Utrecht University, Heidelberglaan 1, 3584 CS Utrecht, The Netherlands
[f] Spinoza Centre for Neuroimaging, Meibergdreef 75, 1105BK, Amsterdam, The Netherlands

ARTICLE INFO

ABSTRACT

Functional MRI enables the acquisition of a retinotopic map that relates regions of the visual field to neural populations in the visual cortex. During such a "population receptive field" (PRF) experiment, stable gaze fixation is of utmost importance in order to correctly link the presented stimulus patterns to stimulated retinal regions and the resulting Blood Oxygen Level Dependent (BOLD) response of the appropriate region within the visual cortex. A method is described that compensates for unstable gaze fixation by recording gaze position via an eyetracker and subsequently modifies the input stimulus underlying the PRF analysis according to the eyetracking measures. Here we show that PRF maps greatly improve when the method is applied to data acquired with either saccadic or smooth eye movements. We conclude that the technique presented herein is useful for studies involving subjects with unstable gaze fixation, particularly elderly patient populations.

Crown Copyright © 2016 Published by Elsevier Inc. All rights reserved.

Introduction

The spatial arrangement of an image is preserved when it passes through the cornea, lens and finally the photoreceptors of the retina, i.e. neighbouring visual field positions have adjacent representation in the retina. While this is not true for the optic nerve fibres (Fitzgibbon and Taylor, 1996; Horton et al., 1979), retinotopy is again present in the lateral geniculate nucleus (LGN). Lesion studies from more than a century ago showed that this mapping is also maintained in the primary visual cortex (V1) (Henschen, 1893; Holmes, 1918; Inoue, 1909).

Magnetic resonance imaging (MRI) enables several approaches for examining the features of the visual system with a high level of detail. Anatomical MRI allowed, in combination with lesion studies, important observations regarding cortical magnification (Horton and Hoyt, 1991) and cortical thickness measures (Fischl and Dale, 2000). Functional MRI (fMRI) of the visual cortex on the other hand allowed for conclusions based on temporal changes of brain metabolism during a given task. These methods have been applied not only in healthy subjects but also in several patient populations, e.g. glaucoma (Duncan et al., 2007; Engin

et al., 2014), age-related macular degeneration (AMD) (Baseler et al., 2011a; Sunness et al., 2004) and other disorders at different levels of the visual system (Barton and Brewer, 2015; Morland et al., 2001; Papanikolaou et al., 2014). MRI methods can be used to study neuroplasticity in the visual cortex (Baseler et al., 2011b) or to complement other modalities in characterizing visual field loss (Papanikolaou et al., 2014).

An early approach to map the visual cortex in detail using fMRI was based on travelling wave paradigms (Engel et al., 1994). The stimuli involved expanding, concentric rings that were presented with flickering checkerboard patterns. When a ring expanded beyond the screen a new ring was created in the centre, thereby creating a periodic stimulus and resulting in a periodic modulation of the BOLD response in the visual cortex. An additional possibility to map the visual cortex is provided by multifocal stimuli where each stimulus segment possesses a different time course and constitutes a regressor of a General Linear Model (GLM) (Vanni et al., 2005). More recently, a new method referred to as *receptive field modelling* became increasingly popular in studies targeting retinotopic mapping and similar applications. As the BOLD signal in a single voxel is influenced by a plethora of neurons (and even if it were possible to measure influences of a single neuron, that neuron would be part of a network and influenced by millions of other neurons) these approaches

are often referred to as *population receptive field (PRF) models* (Wandell and Winawer, 2015). The term *receptive field* was first used to describe a specific region of skin which has to be stimulated in order to evoke a scratch reflex (Sherrington, 1910) and later transferred to vision science by Hartline (1938) where it was defined as the region of the retina which must be illuminated in order to obtain a response in a given fibre. The resulting region corresponds to the receptive field of that fibre. Herein the term *receptive field* is used to establish a connection between a stimulated retinal region and a specific voxel located in the primary visual cortex, which then exhibits an increased BOLD signal.

Population receptive field mapping using fMRI was first presented in 2008 (Dumoulin and Wandell, 2008b). Besides conventional ring and wedge stimuli a flickering bar, moving across the screen in different directions, was also used. Parameters (i.e. position and size) of a hypothesised PRF were then modified until the modelled time series based on the stimulus sequence showed maximum correlation with the real, measured signal of a voxel. Using this information, a voxel's receptive field was modelled as a symmetric, two-dimensional Gaussian.

Since that first study, several groups have presented approaches to refine the PRF stimulation and analysis methods. Eccentricity-scaled bars and simultaneous expanding ring and rotating wedge stimuli (Alvarez et al., 2015) have been proposed and more sophisticated models with additional Gaussian functions increase the detection accuracy of cortical activations by modelling suppressive surround (Zuiderbaan et al., 2012) or nonlinearities (Kay et al., 2013). Other groups proposed methods to reconstruct the PRF without making any a priori assumptions about the PRF shape (Greene et al., 2014; Lee et al., 2013).

But irrespective of the level of sophistication of stimulus or model, all of these experiments critically depend on one additional variable, namely subject compliance.

Excessive head movement and/or unstable gaze fixation precludes any reliable assumptions regarding the experimental paradigm by interfering with the PRF reconstruction, limiting interpretability, or, in the worst case, prohibit PRF construction. This is particularly important in patients, especially elderly patients. Slight head movement can be compensated for by appropriate realignment of the functional images during pre-processing but excessive movement requires the functional run to be repeated.

The control of fixation is more challenging and requires an eyetracker. Since MR-compatible eyetracking was introduced (Felblinger et al., 1996; Gitelman et al., 2000; Kimmig et al., 1999) this method has been increasingly used (Freeman et al., 2011; Herrmann et al., 2010; Kimmig et al., 1999; Visser et al., 2013). Some authors incorporated eyetracker data in real-time to modify visual stimuli (Schilbach et al., 2009; Wilms et al., 2010), but, to date, eyetracking performed during retinotopy has only been used to verify stable fixation (Papanikolaou et al., 2014; Somers et al., 1999).

The present report describes the use of eyetracker measures during the data analysis stage to compensate for unstable fixation during the experiment. Although previously proposed (Dumoulin et al., 2008a), they were only used to simulate effects of potential artefacts caused by eye movements (Klein et al., 2014; Levin et al., 2010) not to correct for unstable fixation. The present study utilises the eyetracker data to modify the assumed stimulation pattern during data analysis of unstable fixation runs and compares the results to PRF maps obtained from stable fixation runs in the same subjects.

Methods

Subjects

Nine healthy subjects (5 females, 4 males, age 26 ± 4.4) with normal visual acuity and no history of significant eye disease were examined on a 3 T Siemens TIM Trio scanner using the lower part of a 32-channel head coil, which itself corresponds to a 20-channel coil. Subjects were recruited from the local university environment and were naïve with

regard to visual experiments. They were introduced to the stimulus only shortly before the measurement and received no further training. All subjects gave written informed consent and all experiments were approved by the local ethics committee.

MRI measurements

Structural images were acquired before functional scanning using a magnetization-prepared rapid gradient-echo (MPRAGE) sequence (TE/TR = 4.21/2300 ms, 160 sagittal slices, voxel size = $1 \times 1 \times 1$ mm^3, field of view = 256 mm). Functional MR images were acquired using the CMRR multiband sequence (Moeller et al., 2010). The effective voxel size was $1 \times 1 \times 1$ mm^3 and TE = 30 ms.

Two different acquisition parameter sets were used to assess the influence of different acquisition parameters on the gaze correction procedure. TR was 1000 ms for the first five subjects (TR1000 group) but 1500 ms for the following four subjects (TR1500 group) accompanied by a reduction in the multiband factor from 3 to 2. Additionally, the number of slices was minimally changed from 27 to 28 and a slice gap of 10% was introduced to minimize interslice interference.

Slices were aligned orthogonally to the calcarine sulcus and covered 27 mm of the occipital cortex for the TR1000 group and 30.8 mm of the occipital cortex for the TR1500 group, starting from the occipital pole.

Stimuli

The visual stimulus used was a modified version of that introduced by Dumoulin and Wandell (2008b) and generated in the Matlab programming environment (The MathWorks, Inc., Natick, Massachusetts) using mrVista (Vista Lab, Stanford University, California). It consisted of a moving bar exposing a checkerboard flickering with a frequency of 8 Hz. The moving bar crossed the screen slowly horizontally and was subsequently rotated by 45° clockwise to cross the screen again. This continued until the bar had travelled across the screen in eight different directions. At each time point, the bar itself covered 12.5% of the available screens' width. As the bar moved slightly after each TR it crossed the screen in 36 s taking 36 discrete steps for TR = 1 s experiments and 24 discrete steps for TR = 1.5 s experiments respectively. The stimulus covered a central area corresponding to 20° visual angle diameter. Thus the bar was 2.5° wide and one step corresponded to 0.56° for TR = 1 s and 0.83° for TR = 1.5 s, respectively. After each diagonal crossing of the bar a mean luminescence screen was presented for 12 s. The total length of one run was therefore 5 min 36 s.

Subjects were instructed to fixate a small spot (with a diameter of 12 pixels i.e. 0.23° visual angle) at the centre of the screen during stimulus presentation. Three different run types were presented, differing with respect to the behaviour of the fixation spot. In the first,

a) Stable
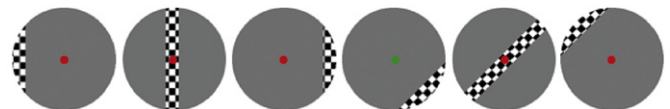
b) Moving (Saccading/Smooth)

Fig. 1. The flickering bar crosses the screen in different directions. During stimulus presentation subjects had to fixate a small spot and report random colour changes. a) For stable runs the spot stayed at the centre of the screen at all times. b) For moving run types however, the spot changed its position at an instant (saccading) or moved around continuously (smooth).
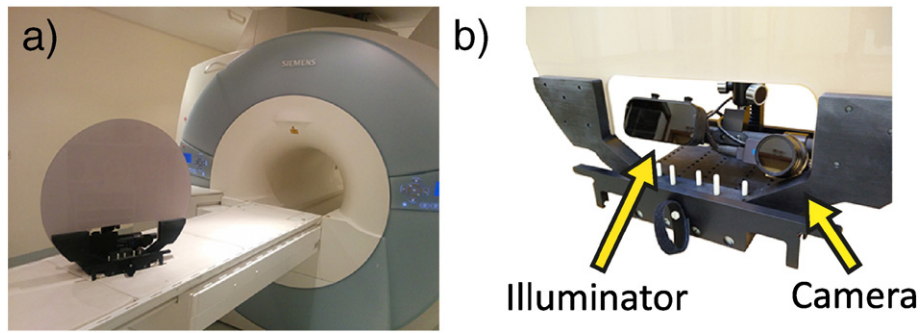
Fig. 2. EyeLink 1000 Plus eyetracker (SR Research, Ottawa, ON) used to record gaze positions at 1000 Hz. The eyetracker is placed at the end of the scanner bore just beneath the screen and consists of an infrared illuminator and an infrared camera.

the fixation spot remained stationary (run type "stable"). In the other two paradigms the spot position was changed randomly every 4 s with either abrupt positional change requiring saccadic eye movement (run type "saccading") or smooth positional change requiring constant gaze readjustment, i.e. smooth pursuit (run type "smooth"). The position of the spot was limited to half the total screen width and height around the centre. To increase attention and assist fixation, subjects had to report a (random) colour change of the fixation spot using a
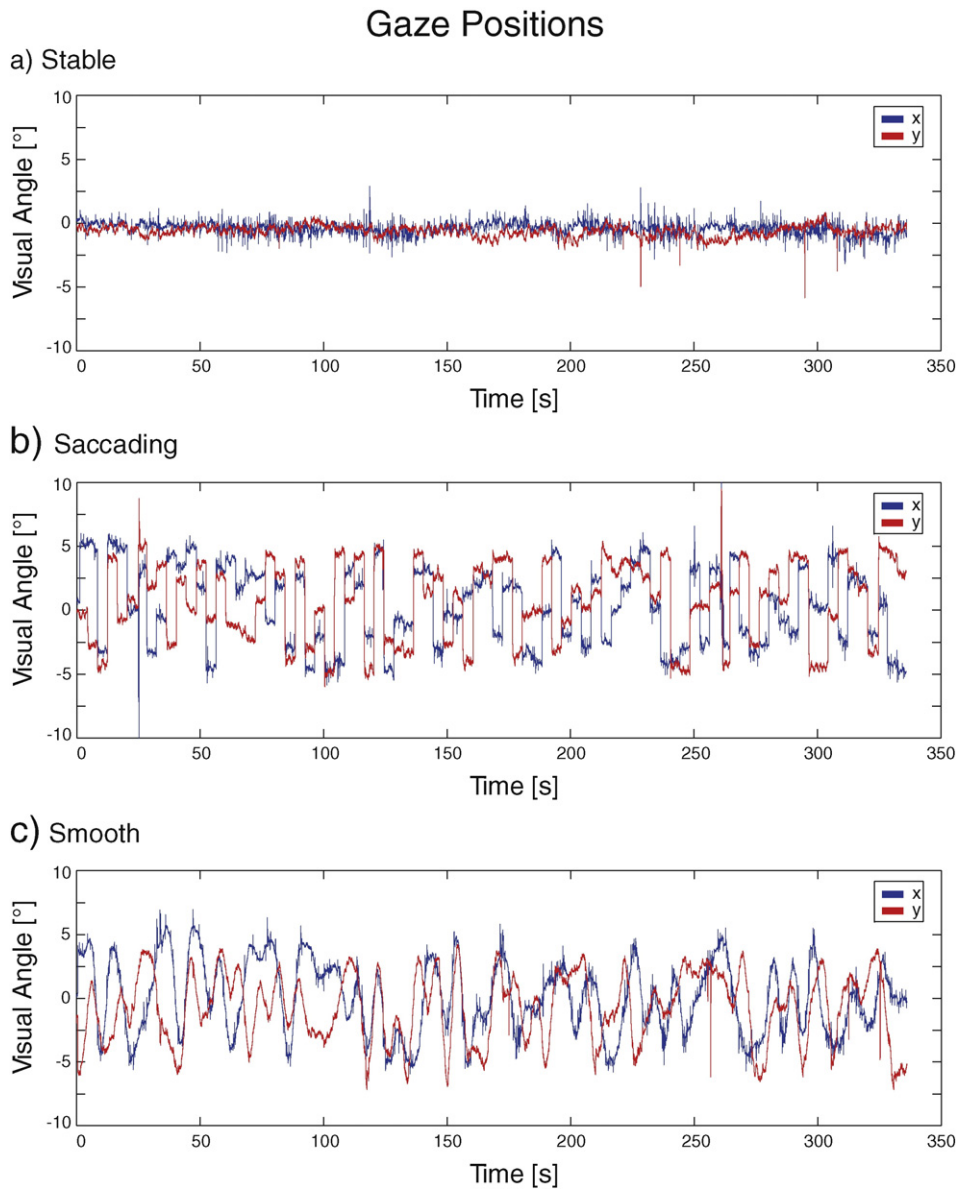
Fig. 3. Eyetracker data of a typical subject for a single run. a) The stable run shows only small, random gaze changes which may origin from microsaccades and tracking inaccuracy. b) The gaze position recorded during a saccading run, on the other hand, follows a pattern corresponding to the sudden position changes of the fixation spot. c) Eyetracker data of a smooth run show similar behaviour but instead of exhibiting saccades the gaze continuously pursues the slowly moving fixation spot.

response pad. Fig. 1 illustrates the difference of the different run types with respect to the presented fixation spot. Two runs were performed for each of the three stimulation types (stable, saccading, smooth) resulting in a total of six retinotopy runs per subject.

Eyetracking

Gaze position data were acquired during each trial with a rate of 1000 Hz using an EyeLink 1000 Plus (SR Research, Ottawa, ON) eyetracker placed at the end of the scanner bore. The eyetracker consists of an infrared illuminator and camera, which records the eye and allows tracking gaze direction using the positions of pupil and cornea reflection (see Fig. 2). The assembly of the eyetracker was slightly modified by placing the infrared illuminator and camera behind the screen. This minimized artefacts due to vibration, which are more prominent near the centre of the bore. This configuration also allowed the use of larger visual angles as the screen was positioned closer to the eye. The tracked eye was chosen by the subjects themselves; four of the nine subjects chose the left eye. The untracked eye of each subject was covered to improve the agreement of perceived visual sensation and eyetracker data. Dark cloth lined the inside of the scanner to reduce reflections from the bore (Stenbacka and Vanni, 2007). Eyetracker data recorded during blinks and artefacts associated with blinks were removed from the datasets by replacing them with interpolated positions based on eyetracker data acquired 250 ms before and after the blink.
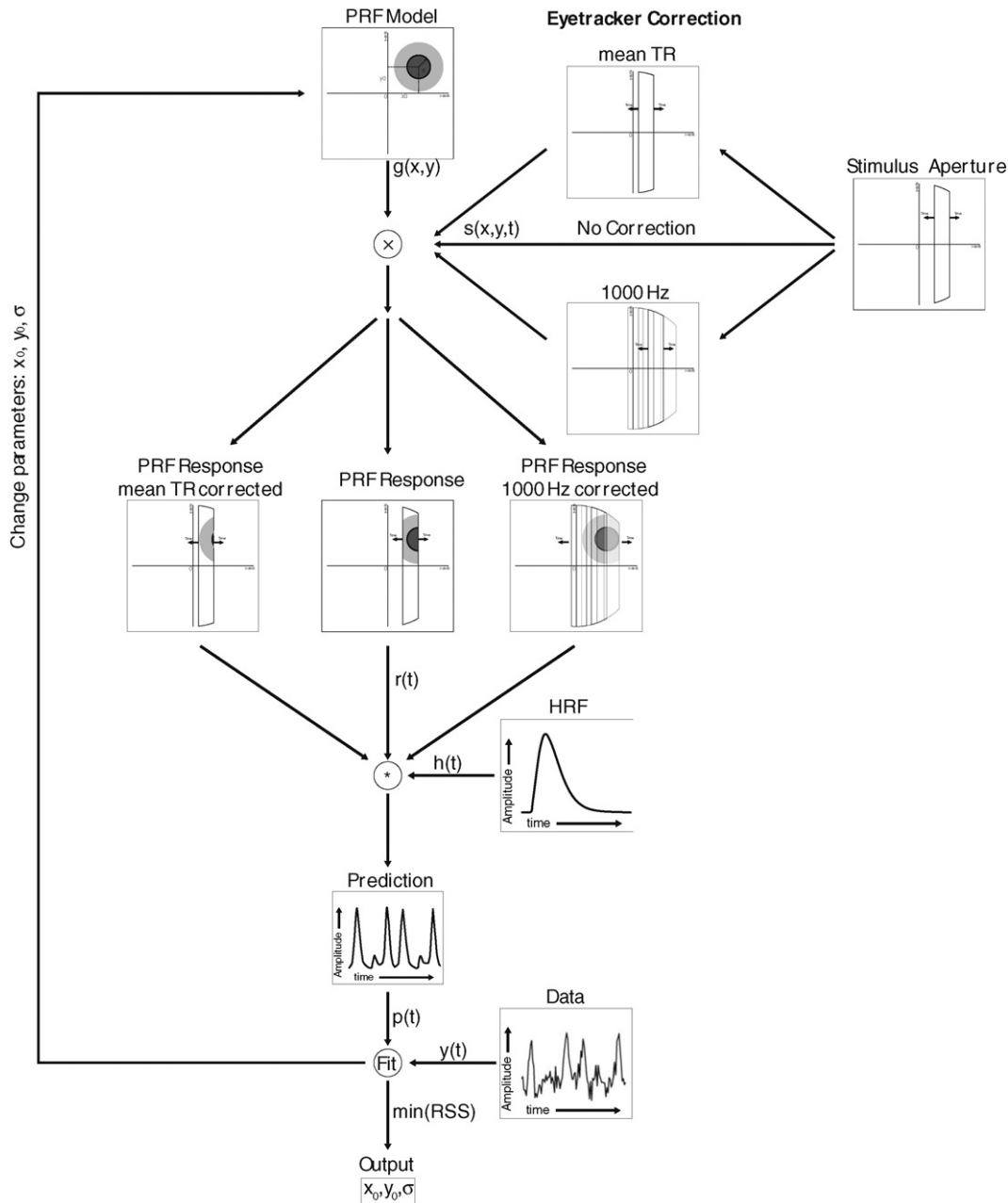
Fig. 4. Adapted from Dumoulin and Wandell (2008b). Eyetracker-based gaze correction modifies the stimulus aperture, and therefore the predicted PRF response, at each point in time based on recorded gaze position data. The modification is done in two different ways. Eyetracker data were either averaged for every TR and then used to shift the stimulus aperture ("mean TR"), or all of the acquired eyetracker data were used by abandoning a binary stimulus aperture and define a gaze density map instead. This results in multiple, simultaneous stimulus apertures with varying opacity for every TR ("1000 Hz"). Modifying the stimulus aperture this way results not in a simple shift, but rather blurs the stimulus aperture based on every gaze position recorded during a TR.
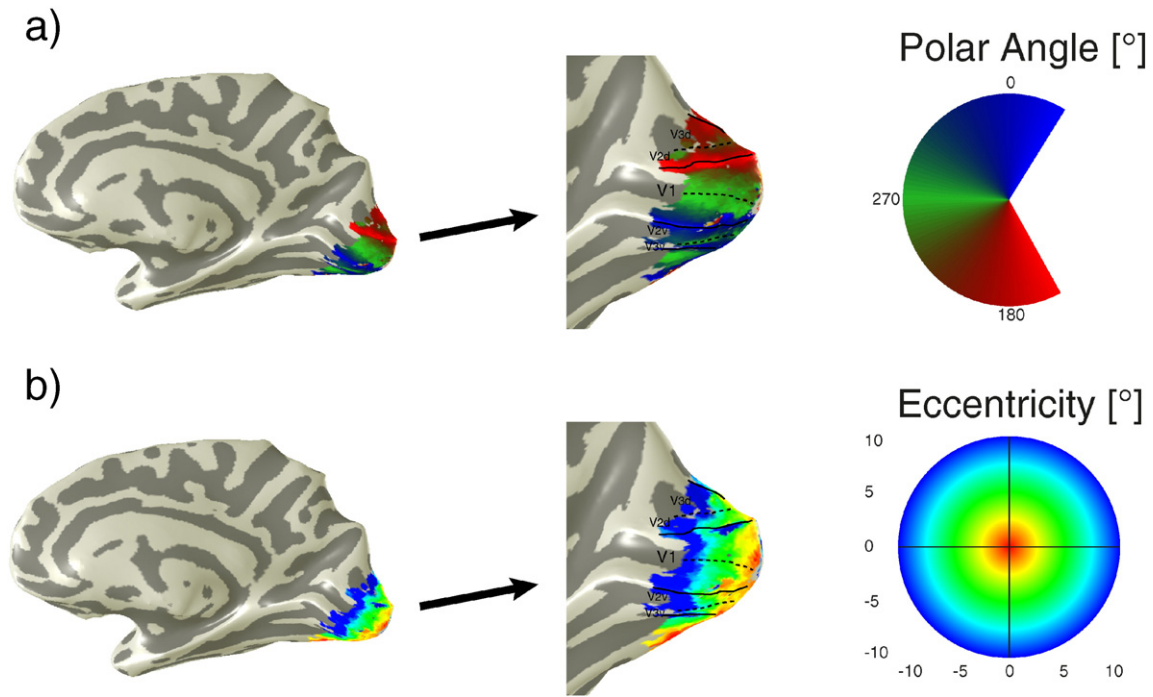
Fig. 5. Results of a subject performing standard retinotopic mapping. V1–V3 are delineated in black. a) Polar angle map. The visual cortex of the right hemisphere corresponds to the left visual field. Phase reversals at the vertical meridian allow for V1–V3 segmentation. b) Eccentricity map. The occipital pole corresponds to central regions of the visual field, while anterior regions of visual cortex correspond to peripheral regions.

Fig. 3 shows eyetracker data measured during the different types of stimuli. As expected, the gaze remains relatively fixed during the stable run. Data of the saccading run show sudden changes of gaze each time the fixation spot switches position. For the slowly moving "smooth" stimulus however, the eye exhibits smooth pursuit rather than saccades which is observed by smooth changes in the graph.

Analysis

Initially, the MPRAGE datasets were segmented using Freesurfer image analysis suite (http://surfer.nmr.mgh.harvard.edu/). The mrVista toolbox (Stanford University, Stanford, CA) implemented in Matlab 7.8 (The MathWorks, Inc., Natick, MA) was used to model the PRF as a two-dimensional Gaussian distribution described by parameters x, y and σ. The PRF model corresponding to a certain voxel is combined with a binary time series, which is equal to one if the flickering bar is present in the assumed PRF of our voxel and zero otherwise, forming the PRF response. Afterwards, the PRF response is convolved with the hemodynamic response function (HRF) which is estimated for each run to predict the BOLD response of the voxel. The ideal PRF parameters (x, y and σ) for each voxel were then identified by minimizing the residual sum of squares between the predicted and observed fMRI time series (Dumoulin and Wandell, 2008b). Although it is frequent practice to average similar fMRI runs before conducting the PRF analysis we processed every run separately to avoid the combination of eyetracker datasets when performing gaze correction.

The gaze position recorded by the eyetracker was used to modify the analysis in two different ways. In the first method ("mean TR") eyetracker gaze data were averaged for every TR. The data were then incorporated in the analysis by shifting the spatial position of the stimulus bar for every TR according to the acquired gaze data. This way the model represents the mean stimulus (i.e. mean bar position) perceived by the subject and not the stimulus which would have been perceived if centre fixation had been perfect.

The second method ("1000 Hz") utilised all the data provided by the eyetracker. Here, no averaging across TR was performed but a gaze density map produced to describe the distribution of gaze during a single TR. Similar to the "mean TR" method the stimulus bar is shifted to a corrected, gaze-dependent position. In contrast to the "mean TR" method however, this is performed for every gaze position that occurred during one TR. The final stimulus image used by the analysis therefore incorporates all modified bars weighted according to the frequency of occurrence depicted in the gaze density map. Thus, the stimulus is no longer binary (as in the "mean TR" method) but rather consists of different bars, each weighted by the duration during which they were perceived by our subject (see Fig. 4).

Evaluation of the correction methods ("mean TR" vs "1000 Hz")

The first and second run of the stable fixation experiment were concatenated for each subject and a PRF analysis (see Methods Section)

Table 1.1
Between-run reliability of the eccentricity parameter: mean absolute error of Run 1 vs Run 2. Statistically significant improvement compared to the uncorrected results are indicated by asterisks (*: p < 0.05).

Visual cortex region	Run type	Uncorrected	Mean TR	1000 Hz
V1	Stable	0.50° ± 0.07°	0.88° ± 0.30°*	0.87° ± 0.31°*
	Stable (demeaned)		0.59° ± 0.09°	0.59° ± 0.08°
	Saccading	1.85° ± 0.44°	0.99° ± 0.24°*	0.98° ± 0.25°*
	Smooth	1.41° ± 0.39°	1.08° ± 0.26°	1.08° ± 0.25°
V2	Stable	0.48° ± 0.07°	0.88° ± 0.31°*	0.87° ± 0.31°*
	Stable (demeaned)		0.58° ± 0.08°	0.57° ± 0.08°
	Saccading	1.77° ± 0.48°	1.02° ± 0.30°*	1.02° ± 0.30°*
	Smooth	1.53° ± 0.42°	1.06° ± 0.27°	1.08° ± 0.26°*
V3	Stable	0.57° ± 0.10°	0.93° ± 0.33°*	0.92° ± 0.33°*
	Stable (demeaned)		0.65° ± 0.25°	0.66° ± 0.23°
	Saccading	1.67° ± 0.56°	0.97° ± 0.22°*	0.99° ± 0.22°*
	Smooth	1.54° ± 0.38°	1.07° ± 0.24°*	1.06° ± 0.23°*

Table 1.2
Between-run reliability of the polar angle parameter: mean absolute error of Run 1 vs Run 2. Statistically significant improvement compared to the uncorrected results are indicated by asterisks (*: p < 0.05).

Visual cortex region	Run type	Uncorrected	Mean TR	1000 Hz
V1	Stable	10.31° ± 2.86°	19.48° ± 9.17°*	19.48° ± 9.74°*
	Stable (demeaned)		11.46° ± 2.86°	11.46° ± 2.86°
	Saccading	29.22° ± 6.88°	24.64° ± 6.88°	24.06° ± 6.30°
	Smooth	30.37° ± 10.89°	24.64° ± 8.02°	24.64° ± 7.45°
V2	Stable	10.89° ± 3.44°	22.92° ± 11.46°*	22.35° ± 11.46°*
	Stable (demeaned)		13.18° ± 4.58°	13.18° ± 4.58°
	Saccading	32.66° ± 8.59°	23.49° ± 8.02°*	22.92° ± 8.02°*
	Smooth	33.80° ± 14.90°	24.64° ± 4.58°*	24.64° ± 4.58°*
V3	Stable	16.62° ± 6.30°	31.51° ± 15.47°*	30.94° ± 14.90°*
	Stable (demeaned)		18.91° ± 5.73°	18.91° ± 5.16°
	Saccading	34.38° ± 10.31°	28.65° ± 10.31°	28.65° ± 9.74°
	Smooth	42.97° ± 21.77°	32.66° ± 10.89°	32.66° ± 12.03°

performed. This long run was formed to offer twice as many time-points to be fitted by the PRF model. The result of the concatenated runs PRF analysis was used to manually define a V1, V2 and V3 ROI for each subject based on phase reversals of the polar angle parameter map, which highlight borders of the visual cortex areas. Fig. 5a shows a polar angle map of a concatenated run with V1–V3 delineated. Analysis was carried out for each of the visual cortex areas separately. Threshold level was set to 10% explained variance, i.e. only voxels where at least 10% of the fMRI signals variance was explained by the PRF model in the concatenated runs were included. The mean absolute error of different parameters (eccentricity, polar angle, PRF size (σ), x, y) was then calculated between the experiments performed during stable and unstable fixation. In detail, the results of the first stable fixation experiments (regarded as ground truth) were compared to the results of the uncorrected first saccading experiments and the uncorrected first smooth experiments. The procedure was repeated for saccading and smooth PRF data incorporating both types of eyetracker-based gaze correction ("mean TR" and "1000 Hz"). The second runs were similarly processed. This yielded twelve mean absolute error results for each subject per visual cortex area and parameter in total. Finally, the mean absolute error results of both runs were averaged.

Table 1.3
Between-run reliability of the PRF size (σ) parameter: mean absolute error of Run 1 vs Run 2. Statistically significant improvement compared to the uncorrected results are indicated by asterisks (*: p < 0.05).

Visual cortex region	Run type	Uncorrected	Mean TR	1000 Hz
V1	Stable	0.55° ± 0.11°	0.65° ± 0.09°	0.65° ± 0.11°
	Stable (demeaned)		0.62° ± 0.09°	0.62° ± 0.11°
	Saccading	1.76° ± 0.51°	0.97° ± 0.14°*	0.93° ± 0.10°*
	Smooth	1.32° ± 0.36°	1.02° ± 0.23°	1.04° ± 0.24°
V2	Stable	0.50° ± 0.09°	0.60° ± 0.09°	0.60° ± 0.10°
	Stable (demeaned)		0.58° ± 0.07°	0.58° ± 0.08°
	Saccading	1.64° ± 0.45°	0.91° ± 0.14°*	0.88° ± 0.15°*
	Smooth	1.36° ± 0.27°	0.96° ± 0.26°*	0.96° ± 0.25°*
V3	Stable	0.56° ± 0.10°	0.66° ± 0.13°	0.66° ± 0.14°
	Stable (demeaned)		0.64° ± 0.12°	0.65° ± 0.12°
	Saccading	1.62° ± 0.38°	1.01° ± 0.16°*	0.99° ± 0.14°*
	Smooth	1.57° ± 0.44°	1.08° ± 0.27°*	1.09° ± 0.30°*
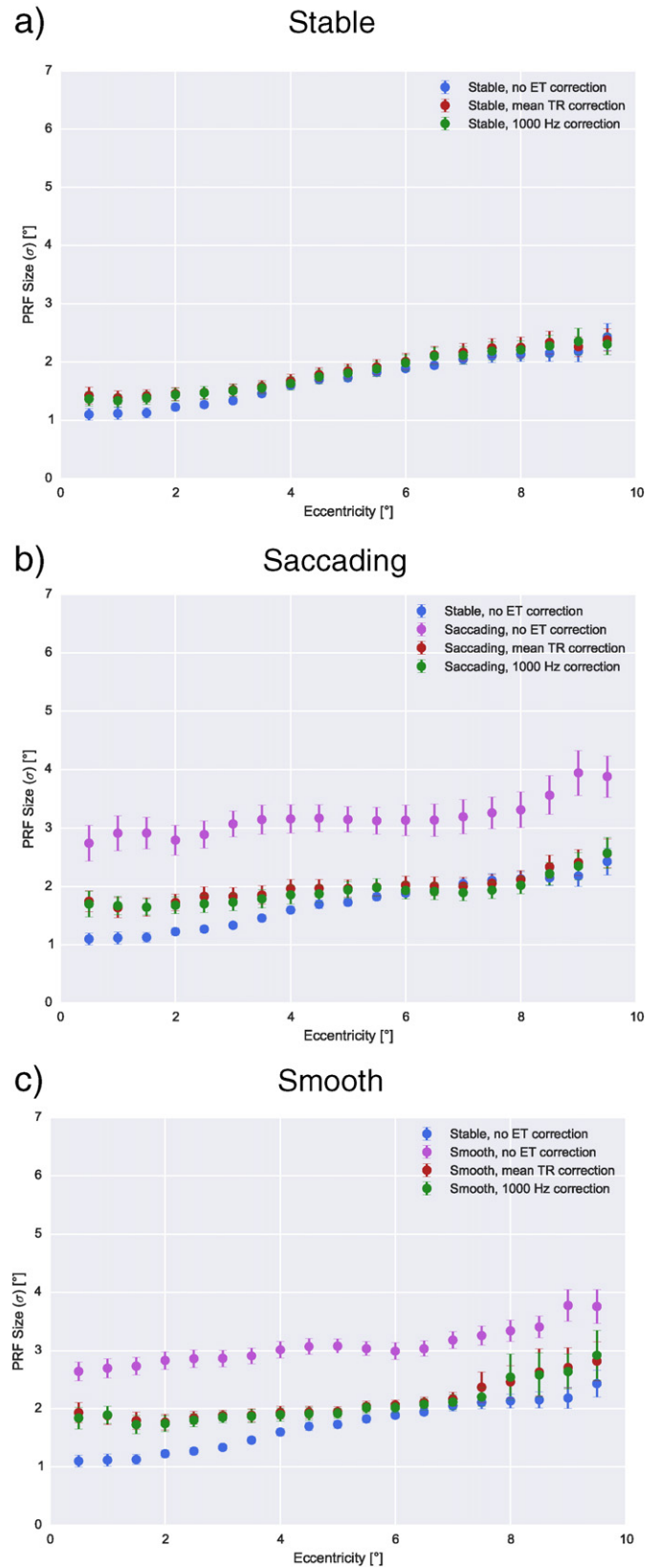
Fig. 6. Plots of PRF size over eccentricity within V1, averaged over all subjects for a) stable, b) saccading and c) smooth runs. Error bars represent the standard error. It can be seen that ET correction greatly improves results from saccading and smooth runs, i.e. deviations to the stable run results are reduced.
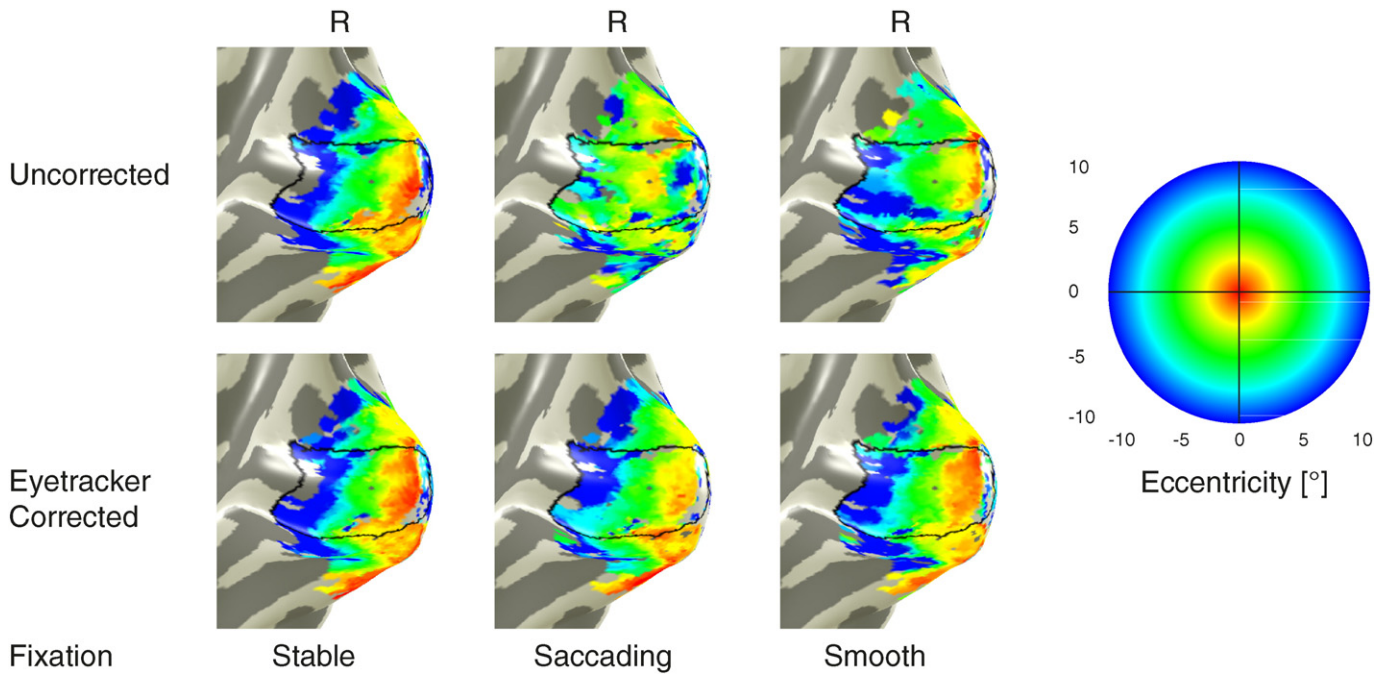
Fig. 7. Uncorrected and "mean TR" corrected eccentricity maps of a single subject for different run types. While eyetracker-based gaze correction hardly affects the eccentricity map of the stable run, the similarity with the stable run increases considerably for the saccading as well as the smooth run after performing the correction.

Results

Successful analysis was achieved for all six runs in eight out of our group of nine subjects, and the retinotopic maps of the single runs with stable fixation show the expected pattern for the PRF parameters. One saccading run of subject #8 had to be excluded due to fatigue causing closure of the palpebral fissure during most of the run (see Fig. S1). Thus, the saccading results of subject #8 are based on a single run only. Fig. 5b shows the results of the eccentricity parameter when performing standard retinotopic mapping using data from a single subject. The eccentricity is minimal near the occipital pole and increases when moving to more anterior regions of the visual cortex. The polar angle parameter allows for the distinction of different regions of the visual cortex by revealing phase reversals occurring at the vertical meridians. As described above, these landmarks were used to define V1–V3 (see Fig. 5a).
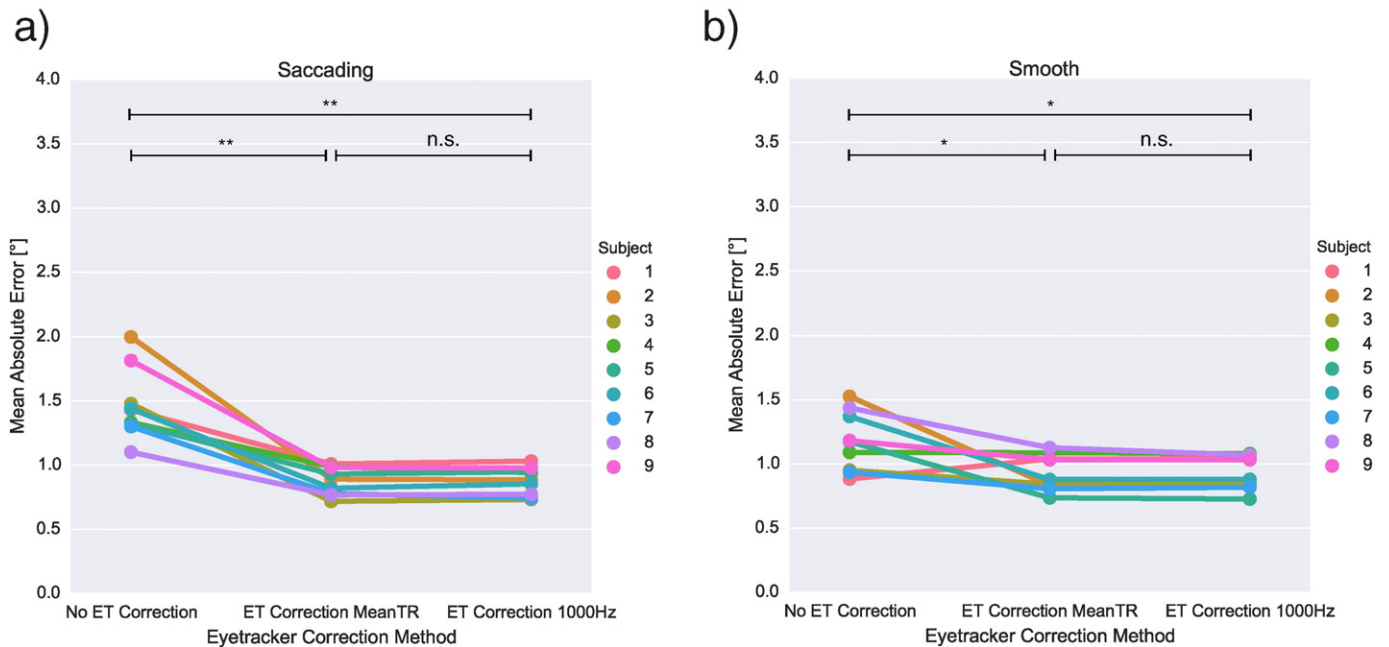
Fig. 8. Comparison of mean absolute error between stable run eccentricity maps and eccentricity maps acquired during a) saccading and b) smooth runs (**: p < 0.01; *: p < 0.05) in V1. Mean absolute errors strongly decrease after applying ET correction. No difference was found between the two ET correction methods "mean TR" and "1000 Hz".

Table 2.1
Mean absolute error of the eccentricity parameter compared to stable runs. Statistically significant improvement compared to the uncorrected results are indicated by asterisks (**: p < 0.01, *: p < 0.05).

Visual cortex region	Run type	Uncorrected	Mean TR	1000 Hz
V1	Saccading	1.47° ± 0.28°	0.88° ± 0.11°**	0.88° ± 0.11°**
	Smooth	1.17° ± 0.23°	0.93° ± 0.14°*	0.93° ± 0.13°*
V2	Saccading	1.41° ± 0.31°	0.87° ± 0.12°**	0.86° ± 0.11°**
	Smooth	1.17° ± 0.24°	0.94° ± 0.15°*	0.93° ± 0.15°*
V3	Saccading	1.47° ± 0.41°	0.90° ± 0.11°**	0.90° ± 0.09°**
	Smooth	1.21° ± 0.25°	0.99° ± 0.18°	0.98° ± 0.17°

Results were highly reproducible; e.g. comparison of the two stable runs yielded a mean absolute error of 0.50° ± 0.07° for V1 eccentricity maps, a mean absolute error of 10.31° ± 2.86° for V1 polar angle maps and a mean absolute error of 0.55° ± 0.11° for V1 PRF size (σ) maps (see Tables 1.1–1.3 for V2 and V3 results and Tables S1.1 and S1.2 for results of the x and y parameters, respectively).

Applying eyetracker correction to the already stable fixation data significantly increases the mean absolute error of V1 eccentricity maps to 0.88° ± 0.30° for the "mean TR" and to 0.87° ± 0.31° for the "1000 Hz" method. Although the eyetracker itself checks for and corrects the centre fixation before each run, an attempt was made to enhance the calibration even further by demeaning, i.e. removing the mean gaze position from the stable eyetracker time series. This reduced the mean absolute error after eyetracker correction to 0.59° ± 0.09° for the "mean TR" and 0.59° ± 0.08° for the "1000 Hz" method and resulted in mean absolute error values, originating from the uncorrected and the eyetracker corrected data, not being significantly different. If fixation can be assumed to exhibit random deviations from the centre, removing the mean eyetracker gaze position can help to improve PRF mapping.

PRF size (σ) over eccentricity

Fig. 6a shows the correlation of the eccentricity and the PRF size (σ) parameter of stable runs averaged over all subjects within the segmented V1 ROI. As expected, areas of the striate cortex corresponding to central regions correspond to small σ, while areas far from the fovea correspond to larger widths. Eyetracker-based gaze (ET) correction of the stable runs only marginally affects the results. Fig. 6b and c show the effect of eyetracker-based gaze correction on PRF size over eccentricity for saccading and smooth runs. Uncorrected data show a clear PRF size offset towards higher PRF sizes for all eccentricities. After applying eyetracker-based gaze correction, however, the curve closely follows the course of the stable runs. As is well known (Dumoulin and Wandell, 2008b), PRF size increases, relative to V1, for visual cortex regions V2 and V3. Apart from that, we observed a similar behaviour in these regions (see Figs. S2 and S3).

Eccentricity parameter

Fig. 7 illustrates the eccentricity parameter results of one subject overlaid on the inflated white matter mesh of the same subject. For illustration purposes, the threshold of variance explained was reduced from 0.1 to 0.01 in this figure. Additionally, to improve orientation, V1 is outlined in black. PRF maps in the "Uncorrected" row correspond to the eccentricity maps calculated by the standard analysis, whereas "Eyetracker Corrected" shows the maps after "mean TR" correction based on eyetracker data (see Fig. 4). Gaze correction has minimal effect on data acquired during stable fixation. However, correction of the data based on unstable gaze (saccading and smooth) clearly improved consistency of the resulting eccentricity maps with regards to the stable gaze run.

Fig. 8 shows the improvement of the eccentricity parameter in the primary visual cortex V1 through gaze correction of each subject in detail. Mean absolute error relative to the stable runs decreases for every subject when considering corrected saccading runs. On average mean absolute error is decreased by about 40%, while the standard deviation over the group is decreased by about 61%.

For the smooth stimulus, the mean absolute error is decreased by about 21%, while the standard deviation over the group is decreased by about 41% for the "mean TR" eyetracker-based gaze correction. Visual cortex areas V2 and V3 show similar improvements (see Figs. S4 and S5). Detailed results are shown in Table 2.1.
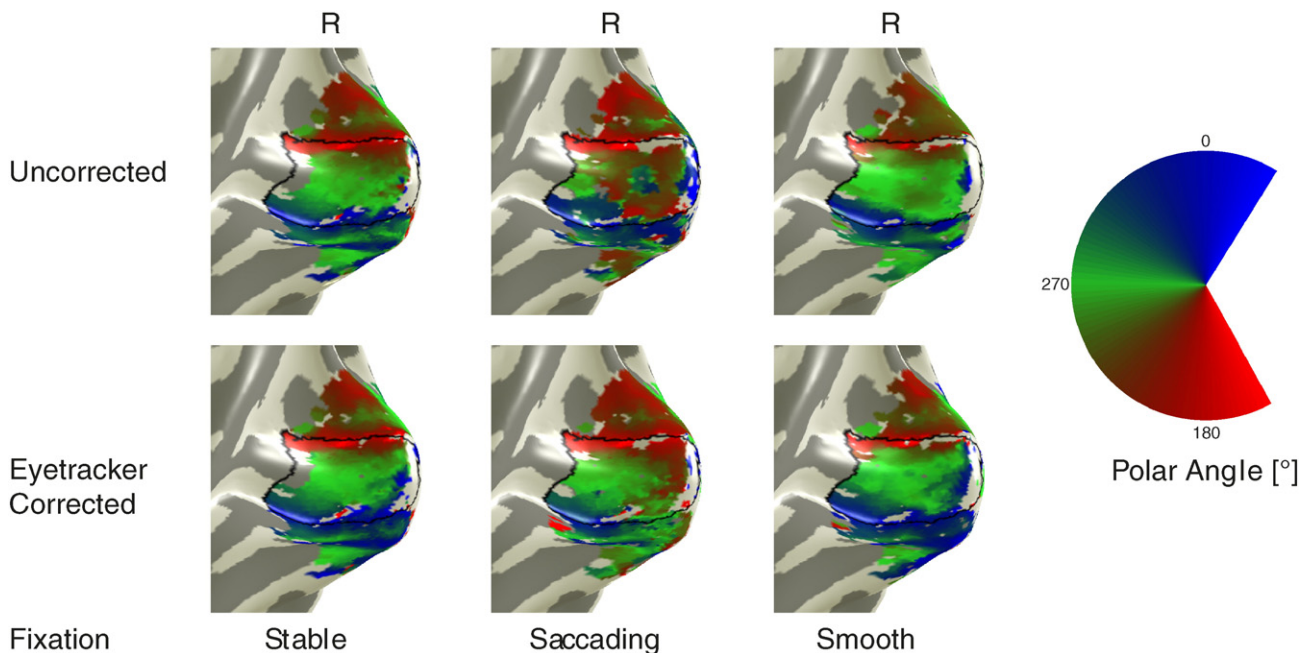
Fig. 9. Uncorrected and "mean TR" corrected polar angle maps of a single subject for different run types. While eyetracker-based gaze correction hardly affects the polar angle map of the stable run, the similarity with the stable run increases considerably for the saccading as well as the smooth run after performing the correction.

Polar Angle - V1
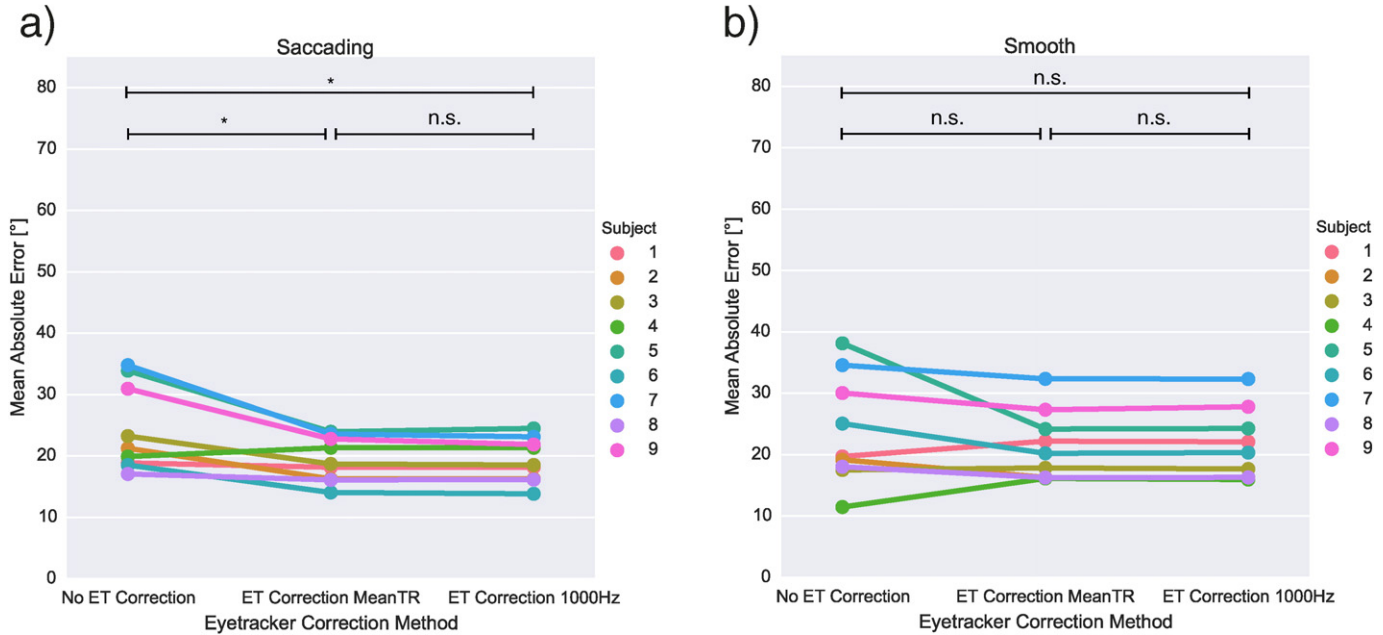
Fig. 10. Comparison of mean absolute error between stable run polar angle maps and polar angle maps acquired during a) saccading and b) smooth runs (*: p < 0.05) in V1. Mean absolute errors between saccading runs and stable runs strongly decrease after applying ET correction. No difference was found between the two ET correction methods "mean TR" and "1000 Hz".

Performance of the two different eyetracker-based gaze correction approaches ("mean TR" and "1000 Hz") was tested using Wilcoxon signed-rank tests. The eccentricity parameter of unstable gaze runs demonstrates significantly reduced difference compared to the stable fixation runs after correction in area V1. Both, the "mean TR" and "1000 Hz" method, exhibit a p-value of $p < 0.01$ when comparing uncorrected and corrected saccading runs and a p-value of $p < 0.05$ when comparing uncorrected and corrected smooth runs ($p < 0.01$, indicated by ** in the figure; $p < 0.05$, indicated by * in the figure).

Polar angle parameter

Similar to Fig. 7, Fig. 9 illustrates the polar angle results of one subject overlaid on the inflated white matter mesh of the same subject. The eyetracker-based gaze correction has minimal effect on data acquired during stable fixation. However, correction of the data based on unstable gaze (saccading and smooth) clearly improved consistency of the resulting polar angle maps with the stable gaze run.

Fig. 10 shows the improvement of the polar angle parameter in the primary visual cortex V1 through gaze correction of each subject in detail. The mean absolute error relative to the stable runs decreases when considering corrected saccading runs. On average, mean absolute error decreased by about 20%, while standard deviation over the group decreased by about 48%. For the smooth stimulus, mean absolute error relative to the stable runs also decreased when performing eyetracker-based gaze correction. On average, mean absolute error decreased by about 10%, while standard deviation decreased by about 35%. Visual cortex areas V2 and V3 also show statistically significant improvements for the saccading runs (see Figs. S6 and S7) Detailed results are shown in Table 2.2.

Detailed results are shown in Table 2.2. Both, the "mean TR" and "1000 Hz" method, exhibit a p-value of $p < 0.05$ (indicated by * in the figure) when comparing uncorrected and corrected saccading runs using Wilcoxon signed-rank tests. However, when comparing uncorrected and corrected smooth runs the differences are not significant ($p > 0.05$, indicated by n.s. in the figure). It has to be kept in mind that

contrary to other parameters, the polar angle mean absolute difference has a maximum value of 180°.

PRF size (σ)

Fig. 11 illustrates the PRF size (σ) results of one subject overlaid on the inflated white matter mesh of the same subject. The eyetracker-based gaze correction has minimal effect on data acquired during stable fixation. However, correction of the data based on unstable gaze (saccading and smooth) clearly improved consistency of the resulting PRF size (σ) angle maps with the stable gaze run.

Fig. 12 shows the improvement of the PRF size (σ) parameter in the primary visual cortex V1 through gaze correction of each subject in detail. Examining the PRF size (σ) in a similar way as the eccentricity parameter, we found that the mean absolute error relative to the stable runs decreased by about 54%, while the standard deviation decreased by about 59% on average for corrected saccading runs. For the smooth stimulus, the mean absolute error decreased by about 39% while the standard deviation decreased by about 29% on average. Visual cortex areas V2 and V3 show similar improvements (see Figs. S8 and S9). Detailed results are shown in Table 2.3.

Using Wilcoxon signed-rank tests, the PRF size (σ) parameter of stable gaze runs also demonstrates significantly reduced mean absolute errors with the unstable fixation run after correction in area V1. Both,

Table 2.2
Mean absolute error of the polar angle parameter compared to stable runs. Statistically significant improvement compared to the uncorrected results are indicated by asterisks (**: p < 0.01, *: p < 0.05).

Visual cortex region	Run type	Uncorrected	Mean TR	1000 Hz
V1	Saccading	24.06° ± 6.88°	19.48° ± 3.44°**	19.48° ± 3.44°**
	Smooth	23.49° ± 8.59°	21.20° ± 5.73°	21.20° ± 5.73°
V2	Saccading	29.22° ± 7.45°	20.63° ± 5.16°***	20.05° ± 4.58°***
	Smooth	25.78° ± 9.17°	21.77° ± 3.44°	21.77° ± 3.44°
V3	Saccading	36.67° ± 12.61°	26.36° ± 7.45°***	26.93° ± 8.02°***
	Smooth	33.80° ± 14.90°	30.37° ± 6.88°	30.37° ± 6.88°
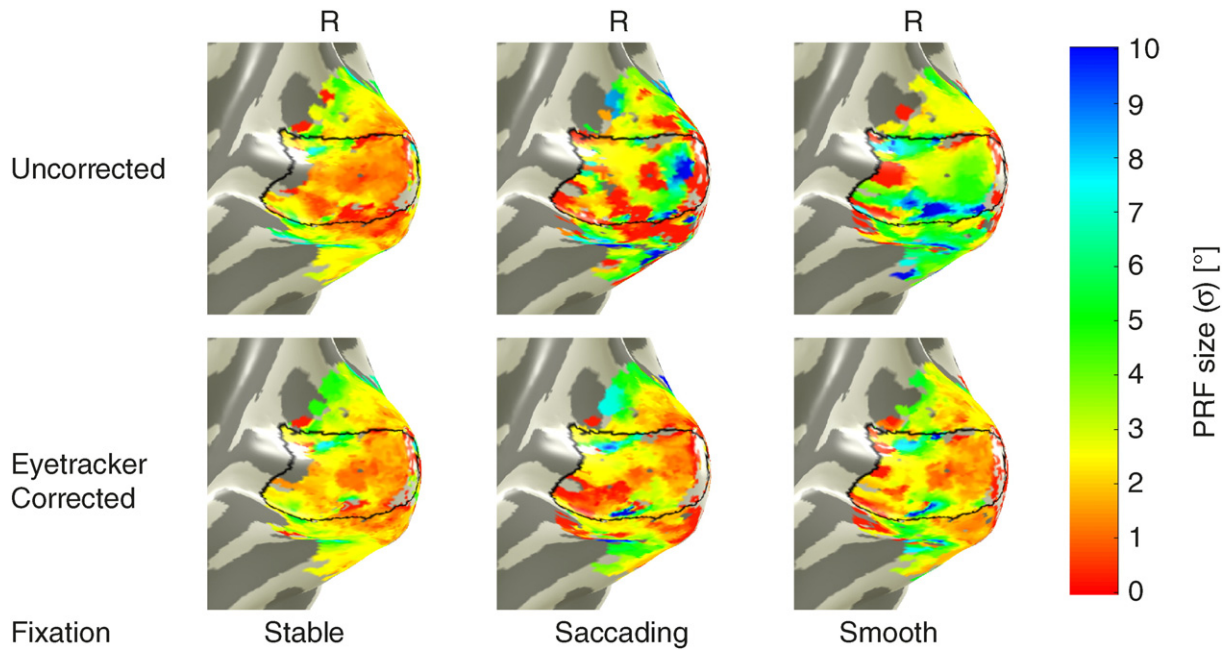
Fig. 11. Uncorrected and "mean TR" corrected PRF size (σ) maps of a single subject for different run types. While eyetracker-based gaze correction hardly affects the PRF size (σ) map of the stable run, the similarity with the stable run increases considerably for the saccading as well as the smooth run after performing the correction.

the "mean TR" and "1000 Hz" method, exhibit a p-value of $p < 0.01$ when comparing uncorrected and corrected saccading runs and a p-value of $p < 0.05$ when comparing uncorrected and corrected smooth runs ($p < 0.01$, indicated by ** in the figure; $p < 0.05$, indicated by * in the figure).

Variance explained

The change of variance explained by the model due to eyetracker correction was also investigated. Fig. 13 illustrates the variance

explained of the subject shown in Fig. 7. Similar to the eccentricity parameter, variance explained increases after eyetracker-based gaze correction for both experiments involving moving fixation spots. Note that in this case the improvement is shown by increased absolute values of explained variance.

Fig. 14 shows the improvement of the variance explained parameter in V1 through gaze correction of each subject in detail. Mean variance explained and its change regarding each run type is displayed. The variance explained increases for every subject in corrected runs, independent of the correction type. The mean explained variance of
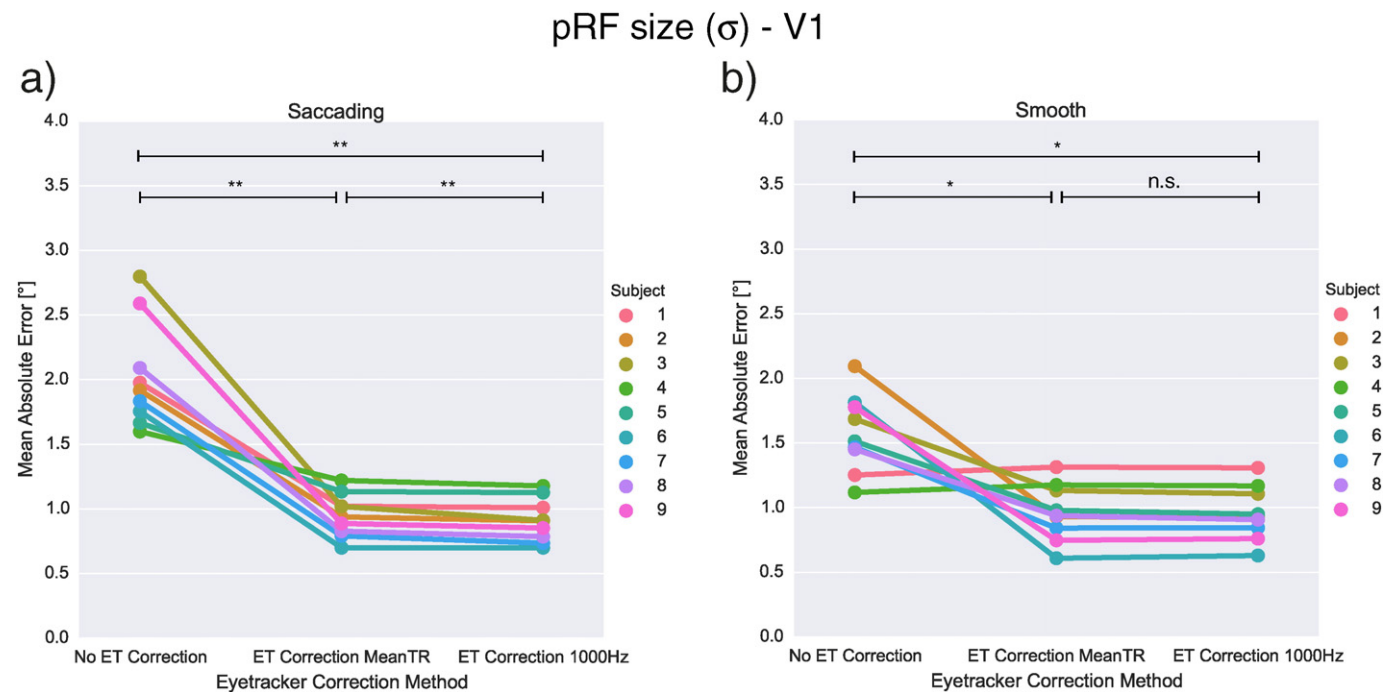
Fig. 12. Comparison of mean absolute error between stable PRF size (σ) maps and PRF size (σ) maps acquired during a) saccading and b) smooth runs (**: $p < 0.01$; *: $p < 0.05$) in V1. Mean absolute errors strongly decrease after applying ET correction. The two ET correction methods "mean TR" and "1000 Hz" were significantly different for saccading runs.

Table 2.3
Mean absolute error of the PRF size (σ) parameter compared to stable runs. Statistically significant improvement compared to the uncorrected results are indicated by asterisks (**: p < 0.01, *: p < 0.05).

Visual cortex region	Run type	Uncorrected	Mean TR	1000 Hz
V1	Saccading	2.02° ± 0.41°	0.95° ± 0.17°**	0.91° ± 0.17°**
	Smooth	1.57° ± 0.30°	0.96° ± 0.22°*	0.96° ± 0.21°*
V2	Saccading	1.85° ± 0.44°	0.81° ± 0.17°**	0.80° ± 0.16°**
	Smooth	1.46° ± 0.29°	0.86° ± 0.23°**	0.85° ± 0.22°**
V3	Saccading	1.85° ± 0.45°	0.91° ± 0.21°**	0.91° ± 0.23°**
	Smooth	1.65° ± 0.33°	0.96° ± 0.21°**	0.96° ± 0.21°**

the saccading runs improved from 10% ± 3% to 13% ± 4% for the "mean TR" and to 13% ± 4% for the "1000 Hz" correction. The mean variance explained also improved for the smooth stimulus. For the "mean TR" as well as the "1000 Hz" correction it rose from 12% ± 2% to 14% ± 3%. The change is significant (p < 0.01, indicated by ** in the figure) when applying Wilcoxon signed-rank tests. Visual cortex areas V2 and V3 show similar improvements (see Figs. S10 and S11). Detailed results are shown in Table 2.4.

Equivalent data and figures concerning the x and y parameters can be found in the supplementary materials (see Figs. S12 to S19).

There was a significant difference in area V1 for the PRF size (σ) parameter (p < 0.01) and the variance explained (p < 0.05) regarding the scope of improvement between the "mean TR" and "1000 Hz" method for saccading runs. There were no other significant differences, regardless of parameter, region and run type.

Also, there was no significant effect of the sequence parameters used, i.e. data from the TR1000 group did not differ significantly from the corresponding TR1500 group data (p > .05).

Discussion

This study describes the use of eyetracker measures during the data analysis stage to account for unstable fixation during fMRI experiments, successfully utilising eyetracker data to modify the assumed stimulation pattern during data analysis and obtaining improved similarity with the PRF maps obtained from stable fixation runs in the same subjects.

The PRF parameter maps of the experiments featuring a randomly moving fixation spot showed strong improvements after performing eyetracker-based gaze correction; the agreement of uncorrected static fixation and moving fixation activation maps is significantly higher following correction procedures. This effect is present for both the saccading and the smooth stimulus. Thus, eyetracker data recorded during a retinotopy experiment can not only be used to control for stable fixation, but also to effectively reverse at least part of the artefacts originating from unstable gaze fixation by modifying the PRF analysis pipeline. There was a reduced group-wise standard deviation of the mean absolute error after eyetracker-based gaze correction and data which were most affected by unstable gaze also benefited the most from the correction; data less affected by artefacts improved to a lesser degree. The eyetracker-based gaze correction not only improved results of the various PRF parameter maps, but also improved the quality of the data, having the strongest impact on the most affected datasets.

Although the proposed "1000 Hz" method is more sophisticated than the "mean TR" method (one drawback of the "mean TR" method is that different combinations of gaze positions during a TR can lead to one and the same mean bar position) data hardly show significant advantages. A hypothesis which suggested improvement only for small eccentricities (covered by smaller PRFs, which may be more sensitive to errors) was also not supported. Overall, this indicates that the "mean TR" method is sufficient for eyetracker-based gaze correction.

The variance explained by the PRF model rises for both the saccading and the smooth stimuli, replicating earlier results (Levin et al., 2010). Therefore, data corrected with the use of eyetracker data not only show more sensible maps but are also more reliable, as the voxel time series exhibit a higher correlation with the stimuli used during analysis.

Dependence of eyetracker-based gaze correction on stimulus type (saccading vs smooth)

Our results demonstrate that data sets containing artefacts originating from instantaneous, saccading gaze changes benefit more from the eyetracker-based correction than data sets with smooth gaze changes. The fact that saccading gaze data generally shows higher errors (due to more variance in gaze position) when compared to smooth runs is
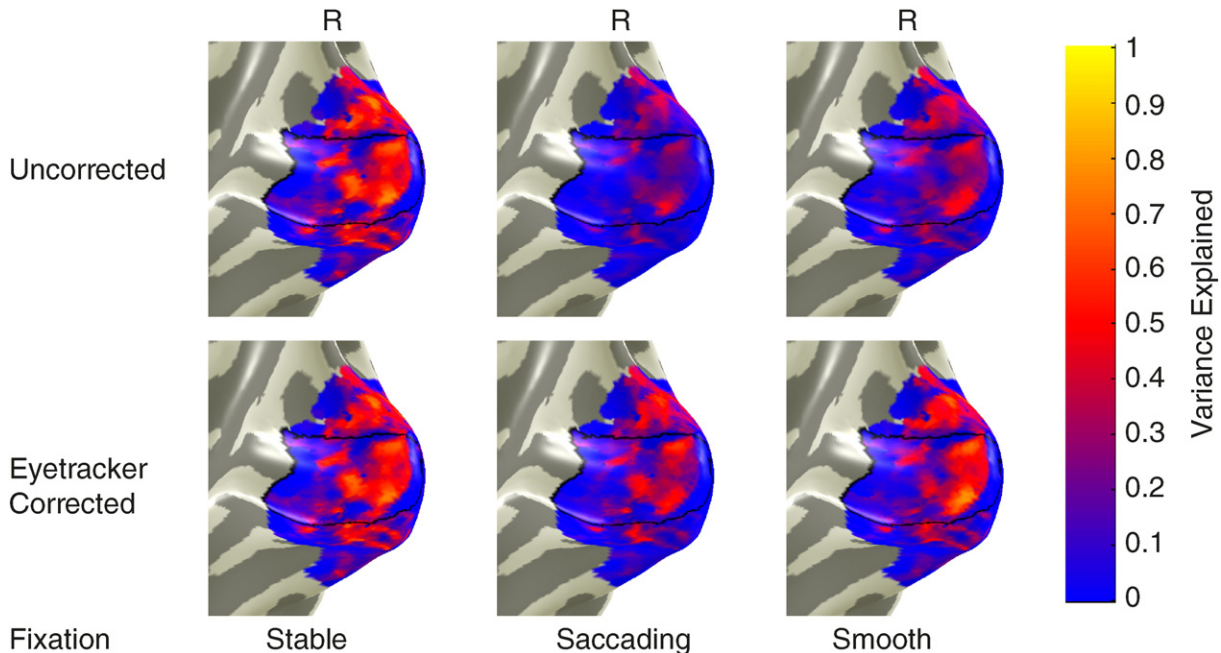
Fig. 13. Uncorrected and "mean TR" corrected maps of variance explained of a single subject for different run types. While eyetracker-based gaze correction hardly affects the variance explained map of the stable run, both, the saccading run as well as the smooth run have their variance explained increased after performing the correction.

Variance Explained - V1
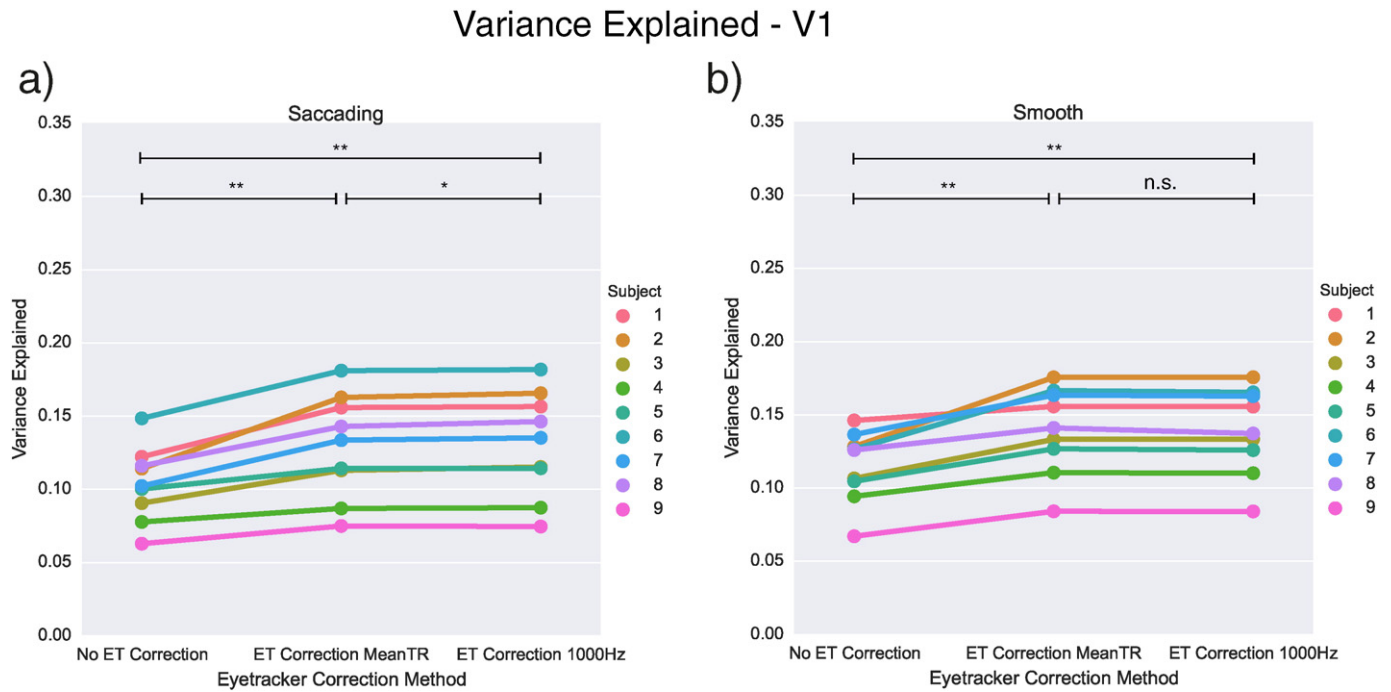
Fig. 14. Comparison of explained variance between stable and a) saccading or b) smooth runs (**: p < 0.01; *: p < 0.05) in V1. Explained variance significantly increases after applying ET correction. The two ET correction methods "mean TR" and "1000 Hz" were significantly different for saccading runs.

compatible with our findings that the more data sets were affected by artefacts the greater the benefits of eyetracker-based correction.

Influence of stimulus frequency on gaze stability

When inspecting eyetracker time series, no systematic eye movements correlating with image acquisition stimulus position changes at the beginning of each repetition time (TR) were apparent. In order to eliminate the possibility that eye movements are affected by stimulus frequency we performed Fourier transformations of the eyetracker signals recorded during stable runs. We then proceeded to average the calculated spectra of all runs (see Fig. S20). No spectral peaks for the frequencies corresponding to TR = 1 s and TR = 1.5 s, respectively, are present, thus, no dependency of eyetracking data on stimulus presentation frequency is indicated.

Attention-related PRF modulation

It has been recently shown (Klein et al., 2014; Puckett and DeYoe, 2015) that PRFs can be modulated by attention. However, in those experiments the subjects were instructed to fixate a central spot while covertly attending peripheral regions. In our setup the subjects were instructed to always focus on the fixation spot. Therefore, in our study attention was always aligned with gaze, regardless of the fixation spot position. Obviously, this is not true for the split second during saccading

runs when subjects searched for the fixation spot after the spot changed position. Compared to the TR, this time window is very small and should therefore not affect our results.

PRF reliability

The data highlight the reliability and robustness of the PRF method combined with high-resolution multiband imaging. The averaging of multiple runs, often applied when investigating PRF maps, was not used because eyetracker datasets are tied to a single run. Each comparison of parameter maps is therefore based on PRF analysis of single five-minute fMRI runs. Additionally, only the tracked eye was stimulated by flickering bars, effectively reducing the extent of visual input. This could be problematic if the estimated PRF maps were to change considerably between runs, but that was not the case as uncorrected stable fixation runs show a very low mean absolute error of 0.50° ± 0.07° for V1 eccentricity maps and similar low values for other PRF parameters.

The two uncorrected runs based on saccading fixation (V1: 1.85° ± 0.44°) and smooth fixation (V1: 1.41° ± 0.39°) feature a randomly moving fixation spot that differed between runs and do not reveal such a high correlation. The application of eyetracker-based gaze correction improved the reproducibility by lowering the mean absolute error of the two runs by about 46% (to 0.99° ± 0.24° for the "mean TR" correction and 0.98° ± 0.25° for the "1000 Hz" correction) in case of the saccading fixation spot and by 23% (1.08° ± 0.26° for the "mean TR" correction and to 1.08° ± 0.25° for the "1000 Hz" correction) in case of the smooth fixation spot. These values are not equivalent to those with stable fixation but demonstrate clear improvement in the reproducibility of PRF maps, which can be highly stable even when gaze fixation is not optimal. A reliable PRF map is therefore easily achievable by conducting a single five-minute scan. Similar improvements concerning reliability, i.e. of the mean absolute errors between the two runs of each parameter, can also be observed for the polar angle and PRF size (σ) parameters in regions V1–V3 (see Tables 1.1– 1.3). The tables also include mean absolute error values of the de-meaned stable runs.

Table 2.4
Change of the explained variance due to eyetracker based gaze correction. Statistically significant improvement compared to the uncorrected results are indicated by asterisks (**: p < 0.01).

Visual cortex region	Run type	Uncorrected	Mean TR	1000 Hz
V1	Saccading	0.10 ± 0.03	0.13 ± 0.04**	0.13 ± 0.04**
	Smooth	0.12 ± 0.02	0.14 ± 0.03**	0.14 ± 0.03**
V2	Saccading	0.11 ± 0.04	0.13 ± 0.04**	0.14 ± 0.04**
	Smooth	0.12 ± 0.04	0.13 ± 0.04**	0.15 ± 0.05**
V3	Saccading	0.11 ± 0.03	0.13 ± 0.04**	0.13 ± 0.04**
	Smooth	0.12 ± 0.04	0.14 ± 0.04**	0.14 ± 0.04**

Limitations

Eyetracker data quality is determined by many factors. The initial calibration links a given number of visual field positions to positions of the pupil and corneal reflection and has consequences on the eyetracker data as other visual field positions are interpolated based on those data. An inaccurate calibration can cause incorrect gaze data and may lead to reduced quality of retinotopic maps if eyetracker-based correction is applied.

Problems can arise during measurement even if calibration is properly performed. As accurate tracking depends upon reflections from the eye, blinks and narrowing of the palpebral fissure can affect the measurements. Blinks can usually easily be removed from the data as they represent very short, distinct events. Narrowing of the palpebral fissure on the other hand can be caused by fatigue and occurs over different timespans and to varying extents. The eyetracker cannot distinguish this from regular gaze and provides erroneous results. It is therefore essential to monitor the subject via the camera image provided by the eyetracker; as only this way one can determine the true reliability of the data. For example, subject #8 showed an increased mean absolute error between the stable and the saccading runs after eyetracker correction, attributable to fatigue-related narrowing of the palpebral fissure during the first run of the saccading stimulus resulting in poor eyetracker data. The effects are striking when examining different parameters and ROIs, e.g. the eccentricity parameter in area V3. The mean absolute error between the stable run and the uncorrected first saccading run was 1.08°, while it amounted to 1.24° for the second one. After applying "mean TR" eyetracker correction, the coefficient rose to 2.34° for the first run, while dropping to 0.94° for the second one, highlighting the poor quality of the acquired eyetracker data during the first run.

Future directions

Mapping results can become more reliable when moving to higher field strengths, and it would therefore be of potential value to implement eyetracking and gaze correction methods using 7 T MRI systems (Hoffmann et al., 2009; Wandell and Winawer, 2011). Eyetracker-based gaze correction could also be combined with other methods, such as correcting for spatial distortions using fieldmaps (Vasseur et al., 2010) or applied to different stimuli, such as simultaneous expanding ring and rotating wedge stimuli (Alvarez et al., 2015) or multifocal stimuli (Vanni et al., 2005), and different PRF models, such as the centre-surround model consisting of two Gaussians (Zuiderbaan et al., 2012). Compensating for unstable fixation could also help with patients who struggle with stable fixation due to central scotomata (e.g. Stargardt disease or AMD patients) or with children possessing only short attention spans.

Some fMRI experiments have used modified visual stimuli based on the actual subjects' gaze direction (Schilbach et al., 2009; Wilms et al., 2010), and this could be applied to retinotopic mapping as well. By modifying or delaying the presented stimulus (e.g. bar position) during the experiment, it is possible to immediately account for unstable gaze fixation with the advantage that this type of correction is independent of the analysis method used and no additional steps have to be added to the analysis.

Conclusion

When correctly acquired, eyetracking data can be used to perform gaze correction improving the accuracy of retinotopy experiments; PRF parameters of the stable gaze fixation experiments show decreased mean absolute error values with the unstable gaze fixation experiments when eyetracker-based gaze correction was applied. Additionally, variance explained is also improved after correction, suggesting that artefacts caused by unstable gaze fixation in PRF mapping of V1–V3 are at least partly reversible, which may help to improve data quality in studies involving patient populations. As positive effects of eyetracker-based correction were most pronounced for data strongly influenced by unstable fixation, these are also the situations one can benefit the most from the proposed method.

Supplementary data to this article can be found online at http://dx.doi.org/10.1016/j.neuroimage.2016.07.003.

References

Alvarez, I., De Haas, B.A., Clark, C.A., Rees, G., Schwarzkopf, D.S., 2015. Comparing different stimulus configurations for population receptive field mapping in human fMRI. Front. Hum. Neurosci. 9.

Barton, B., Brewer, A.A., 2015. fMRI of the rod scotoma elucidates cortical rod pathways and implications for lesion measurements. Proc. Natl. Acad. Sci. U. S. A. 112, 5201–5206.

Baseler, H.A., Gouws, A., Crossland, M.D., Leung, C., Tufail, A., Rubin, G.S., Morland, A.B., 2011a. Objective visual assessment of antiangiogenic treatment for wet age-related macular degeneration. Optom. Vis. Sci. 88, 1255–1261.

Baseler, H.A., Gouws, A., Haak, K.V., Racey, C., Crossland, M.D., Tufail, A., Rubin, G.S., Cornelissen, F.W., Morland, A.B., 2011b. Large-scale remapping of visual cortex is absent in adult humans with macular degeneration. Nat. Neurosci. 14, 649–655.

Dumoulin, S.O., Wandell, B.A., 2008b. Population receptive field estimates in human visual cortex. NeuroImage 39, 647–660.

Dumoulin, S.O., Masuda, Y., Horiguchi, H., Dougherty, R.F., Prakash, S., Liao, Y.J., Wandell, B.A., 2008a. Visual Field Maps in a Subject without an Optic Chiasm. ECVP, p. 44.

Duncan, R.O., Sample, P.A., Weinreb, R.N., Bowd, C., Zangwill, L.M., 2007. Retinotopic organization of primary visual cortex in glaucoma: comparing fMRI measurements of cortical function with visual field loss. Prog. Retin. Eye Res. 26, 38–56.

Engel, S.A., Rumelhart, D.E., Wandell, B.A., Lee, A.T., Glover, G.H., Chichilnisky, E.J., Shadlen, M.N., 1994. fMRI of human visual cortex. Nature 369, 525.

Engin, K.N., Yemişci, B., Bayramoğlu, S.T., Güner, N.T., Özyurt, O., Karahan, E., Öztürk, C., Çağatay, P., 2014. Structural and functional evaluation of glaucomatous neurodegeneration from eye to visual cortex using 1.5 T MR imaging: a pilot study. J. Clin. Exp. Ophthalmol. 5, 341.

Felblinger, J., Muri, R.M., Ozdoba, C., Schroth, G., Hess, C.W., Boesch, C., 1996. Recordings of eye movements for stimulus control during fMRI by means of electro-oculographic methods. Magn. Reson. Med. 36, 410–414.

Fischl, B., Dale, A.M., 2000. Measuring the thickness of the human cerebral cortex from magnetic resonance images. Proc. Natl. Acad. Sci. U. S. A. 97, 11050–11055.

Fitzgibbon, T., Taylor, S.F., 1996. Retinotopy of the human retinal nerve fibre layer and optic nerve head. J. Comp. Neurol. 375, 238–251.

Freeman, J., Brouwer, G.J., Heeger, D.J., Merriam, E.P., 2011. Orientation decoding depends on maps, not columns. J. Neurosci. 31, 4792–4804.

Gitelman, D.R., Parrish, T.B., LaBar, K.S., Mesulam, M.M., 2000. Real-time monitoring of eye movements using infrared video-oculography during functional magnetic resonance imaging of the frontal eye fields. NeuroImage 11, 58–65.

Greene, C.A., Dumoulin, S.O., Harvey, B.M., Ress, D., 2014. Measurement of population receptive fields in human early visual cortex using back-projection tomography. J. Vis. 14.

Hartline, H.K., 1938. The response of single optic nerve fibers of the vertebrate eye to illumination of the retina. Am. J. Phys. 121, 400–415.

Henschen, S.E., 1893. On the Visual Path and Centre.

Herrmann, K., Montaser-Kouhsari, L, Carrasco, M., Heeger, D.J., 2010. When size matters: attention affects performance by contrast or response gain. Nat. Neurosci. 13, 1554–1559.

Hoffmann, M.B., Stadler, J., Kanowski, M., Speck, O., 2009. Retinotopic mapping of the human visual cortex at a magnetic field strength of 7 T. Clin. Neurophysiol. 120, 108–116.

Holmes, G., 1918. Disturbances of visual orientation. Br. J. Ophthalmol. 2, 449–468.

Horton, J.C., Hoyt, W.F., 1991. The representation of the visual field in human striate cortex. A revision of the classic Holmes map. Arch. Ophthalmol. 109, 816–824.

Horton, J.C., Greenwood, M.M., Hubel, D.H., 1979. Non-retinotopic arrangement of fibres in cat optic nerve. Nature 282, 720–722.

Inoue, T., 1909. Die Sehstörungen bei Schussverletzungen der Kortikalen Sehsphäre, nach Beobachtungen an Verwundeten der Letzten Japanischen Kriege. Engelmann, Leipzig.

Kay, K.N., Winawer, J., Rokem, A., Mezer, A., Wandell, B.A., 2013. A two-stage cascade model of BOLD responses in human visual cortex. PLoS Comput. Biol. 9, e1003079.

Kimmig, H., Greenlee, M.W., Huethe, F., Mergner, T., 1999. MR-eyetracker: a new method for eye movement recording in functional magnetic resonance imaging. Exp. Brain Res. 126, 443–449.

Klein, B.P., Harvey, B.M., Dumoulin, S.O., 2014. Attraction of position preference by spatial attention throughout human visual cortex. Neuron.

Lee, S., Papanikolaou, A., Logothetis, N.K., Smirnakis, S.M., Keliris, G.A., 2013. A new method for estimating population receptive field topography in visual cortex. NeuroImage 81, 144–157.

Levin, N., Dumoulin, S.O., Winawer, J., Dougherty, R.F., Wandell, B.A., 2010. Cortical maps and white matter tracts following long period of visual deprivation and retinal image restoration. Neuron 65, 21–31.

Moeller, S., Yacoub, E., Olman, C.A., Auerbach, E., Strupp, J., Harel, N., Ugurbil, K., 2010. Multiband multislice GE-EPI at 7 T, with 16-fold acceleration using partial parallel imaging with application to high spatial and temporal whole-brain fMRI. Magn. Reson. Med. 63, 1144–1153.

Morland, A.B., Baseler, H.A., Hoffmann, M.B., Sharpe, L.T., Wandell, B.A., 2001. Abnormal retinotopic representations in human visual cortex revealed by fMRI. Acta Psychol. 107, 229–247.

Papanikolaou, A., Keliris, G.A., Papageorgiou, T.D., Shao, Y., Krapp, E., Papageorgiou, E., Stingl, K., Bruckmann, A., Schiefer, U., Logothetis, N.K., Smirnakis, S.M., 2014. Population receptive field analysis of the primary visual cortex complements perimetry in patients with homonymous visual field defects. Proc. Natl. Acad. Sci. U. S. A. 111, E1656–E1665.

Puckett, A.M., DeYoe, E.A., 2015. The attentional field revealed by single-voxel modeling of fMRI time courses. J. Neurosci. 35, 5030–5042.

Schilbach, L., Wilms, M., Eickhoff, S.B., Romanzetti, S., Tepest, R., Bente, G., Shah, N.J., Fink, G.R., Vogeley, K., 2009. Minds made for sharing: initiating joint attention recruits reward-related neurocircuitry. J. Cogn. Neurosci. 22, 2702–2715.

Sherrington, C.S., 1910. Flexion-reflex of the limb, crossed extension-reflex, and reflex stepping and standing. J. Physiol. 40, 28–121.

Somers, D.C., Dale, A.M., Seiffert, A.E., Tootell, R.B.H., 1999. Functional MRI reveals spatially specific attentional modulation in human primary visual cortex. Proc. Natl. Acad. Sci. U. S. A. 96, 1663–1668.

Stenbacka, L., Vanni, S., 2007. Central luminance flicker can activate peripheral retinotopic representation. NeuroImage 34, 342–348.

Sunness, J.S., Liu, T., Yantis, S., 2004. Retinotopic mapping of the visual cortex using functional magnetic resonance imaging in a patient with central scotomas from atrophic macular degeneration. Ophthalmology 111, 1595–1598.

Vanni, S., Henriksson, L., James, A.C., 2005. Multifocal fMRI mapping of visual cortical areas. NeuroImage 27, 95–105.

Vasseur, F., Delon-Martin, C., Bordier, C., Warnking, J., Lamalle, L., Segebarth, C., Dojat, M., 2010. fMRI retinotopic mapping at 3 T: benefits gained from correcting the spatial distortions due to static field inhomogeneity. J. Vis. 10, 1–17.

Visser, R.M., Scholte, H.S., Beemsterboer, T., Kindt, M., 2013. Neural pattern similarity predicts long-term fear memory. Nat. Neurosci. 16, 388–390.

Wandell, B.A., Winawer, J., 2011. Imaging retinotopic maps in the human brain. Vis. Res. 51, 718–737.

Wandell, B.A., Winawer, J., 2015. Computational neuroimaging and population receptive fields. Trends Cogn. Sci.

Wilms, M., Schilbach, L., Pfeiffer, U., Bente, G., Fink, G.R., Vogeley, K., 2010. It's in your eyes—using gaze-contingent stimuli to create truly interactive paradigms for social cognitive and affective neuroscience. Soc. Cogn. Affect. Neurosci. 5, 98–107.

Zuiderbaan, W., Harvey, B.M., Dumoulin, S.O., 2012. Modeling center-surround configurations in population receptive fields using fMRI. J. Vis. 12, 10.